I. Physics of Gamma-ray Spectroscopy Measurements

Richard B. Firestone
Lawrence Berkeley National Laboratory, Berkeley, CA 94720 USA

Lecture presented at the Workshop on Nuclear Data for Activation Analysis,
7-18 March 2005, Trieste, Italy

I. Introduction

Gamma-ray spectroscopy plays a fundamental role in both the standardization and implementation of Activation Analysis. Understanding the physics behind gamma-ray measurement and interpretation is important for estimating the accuracy of the NAA application. In this lecture I will discuss how gamma rays interact with matter and how this affects are choice of detectors. I will also discuss how gamma-ray data and other information from various sources can be combined with data to currently used in NAA to determine improved k_0 values.

II. Interaction of Gamma-rays with Matter

There are four main interaction processes.

A. Photoelectric ejection - process in which an atom absorbs a photon and emits an electron as shown in Figure 1. Most important at low energies.

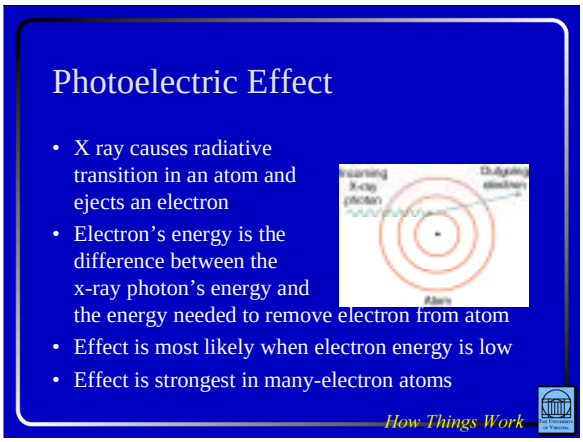

Figure 1

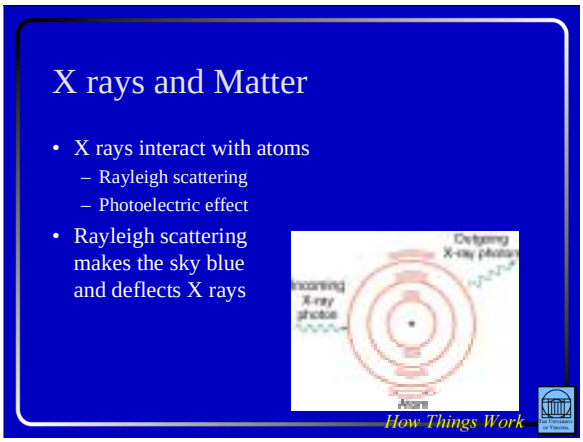

Figure 2

B. Coherent (Rayleigh) scattering – process in which a photon is deflected by the atomic electrons with no loss of energy as shown in Figure 2. Important at low energies.

C. Incoherent (Compton) scattering – process in which a photon is scattered by the atomic electrons with transfer of momentum and energy sufficient to put the electron into an unbound state as shown in Figure 3. This is the main process from 0.2 to 5 MeV.

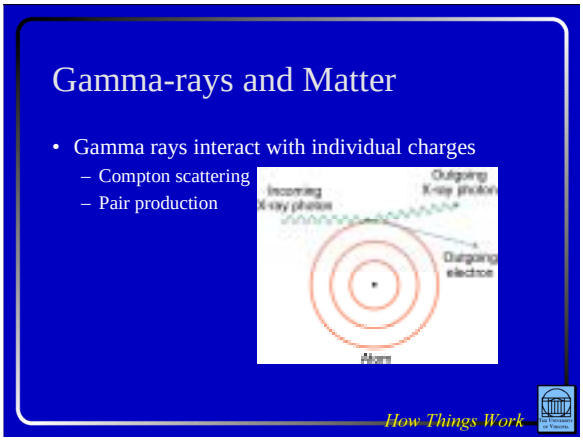

Figure 3

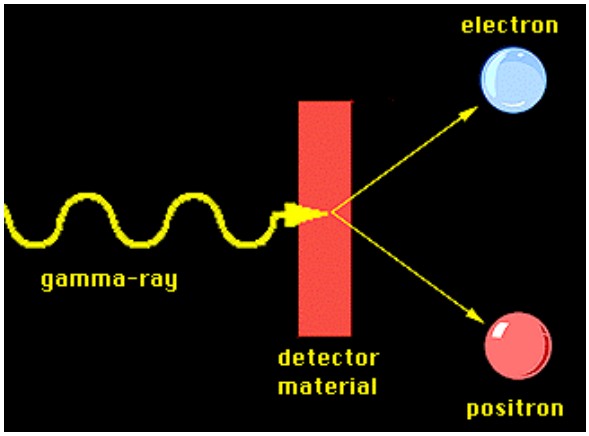

Figure 4

D. Pair production – creation, in the field of the charged particle, of a positron and electron pair as shown in Figure 4. Important at high energy. The electron produces bremsstrahlung radiation and ionization, and the positron is eventually annihilated producing both 511-keV photons and annihilation–in-flight radiation.

The relative cross sections for these processes in Germanium were calculated with the computer code XCOM[1] and are shown in Figure 5.

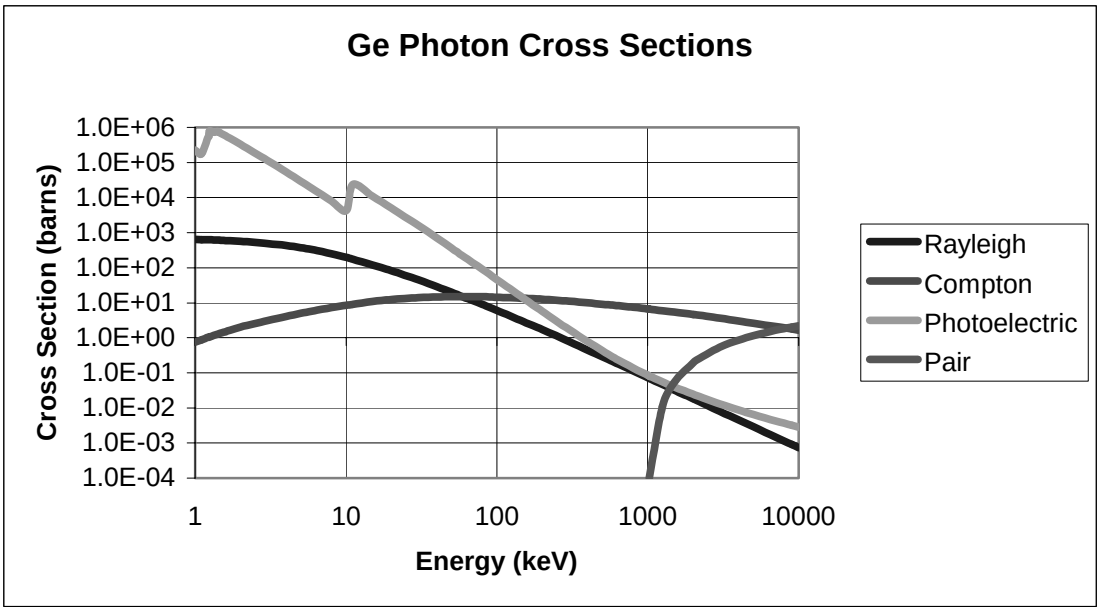

Figure 5. Gamma-ray Interaction cross sections in Germium[1]

III. Gamma-ray Detectors

A. Scintillators – When a γ-ray interacts with a scintillator, it produces a pulse of light, which is converted to an electric pulse by a photomultiplier tube. The photomultiplier consists of a photocathode, a focusing electrode and 10 or more dynodes that multiply the number of electrons striking them several times each. A chain of resistors typically located in a plug-on tube base assembly biases the anode and dynodes. See Figure 6.

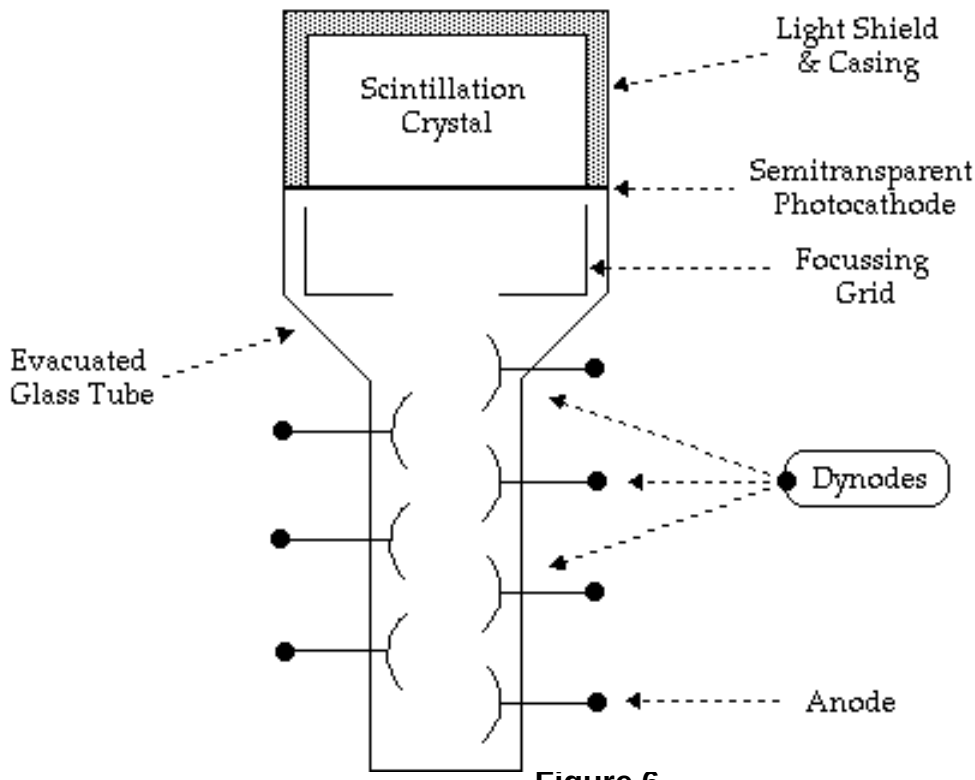

Figure 6

Good scintillation detectors are transparent, have a large light output that is proportional to gamma ray energy, and are available in large size. Commonly available scintillators include thallium activated NaI and CsI crystals, bismuth germinate (BGO), and a wide variety of plastics. NaI is the dominant material for gamma detection because it is well characterized, provides good γ-ray resolution, and is economical. Plastic scintillaors have much faster pulse light decay and are useful in timing applications, but they offer poor energy resolution.

1. NaI(Tl) Scintillation Detectors

The high atomic number for iodine in NaI(Tl) gives good efficiency for γ-ray detection. A small amount of Tl is added in order to shift the wavelength of the scintillation photons so they are not re-absorbed by the crystal. The best resolution is $\approx$50 keV at 662 keV for a 3 inch diameter by 3 inch long cylindrical crystal, and is slightly worse for smaller and larger sizes. Figure 7 shows the

absorption efficiencies of various thicknesses of NaI crystals, and Figure 8 shows the transmission coefficient through the most commonly used entrance windows.

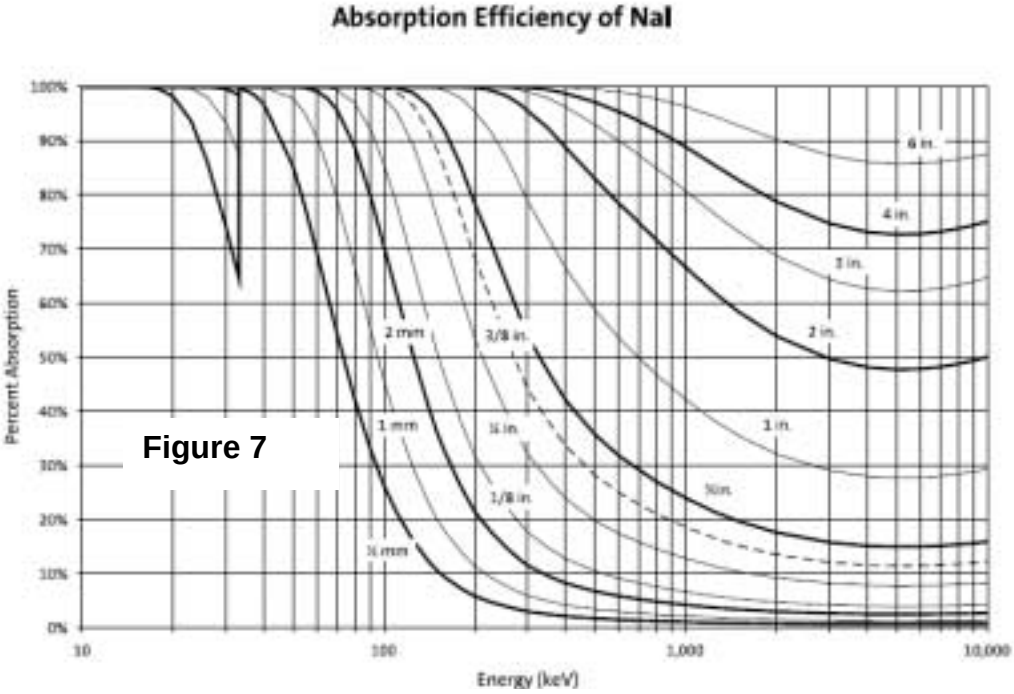

Figure 7

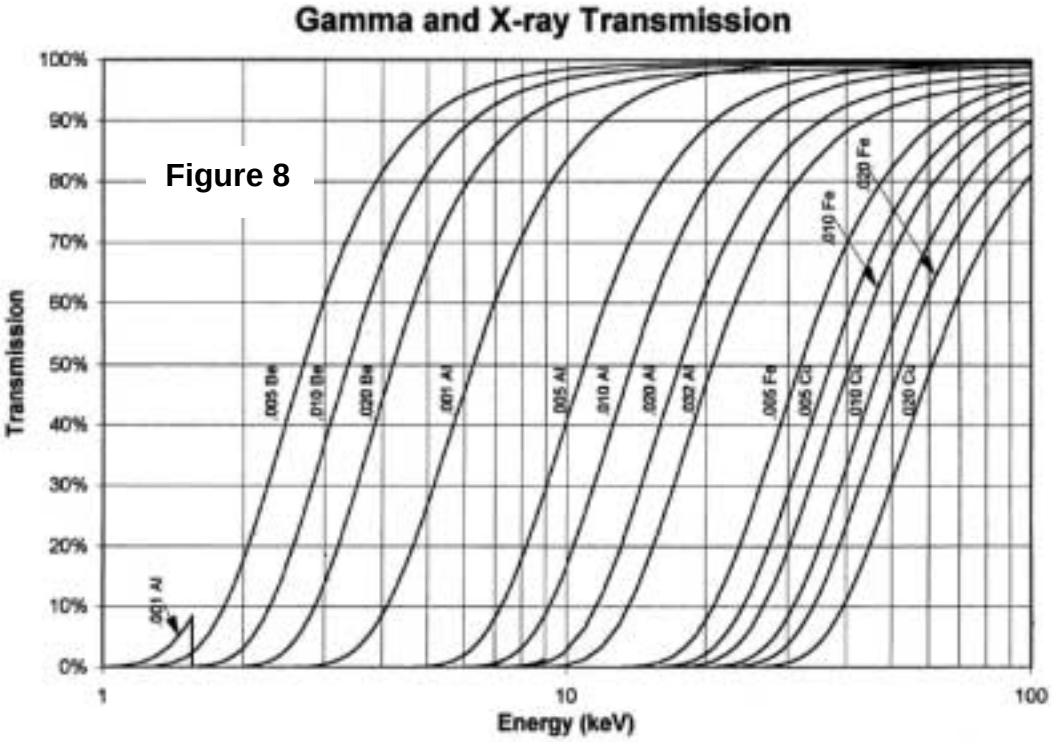

Figure 8

A typical NaI(Tl) spectrum is shown in Figure 9. Many configurations of NaI detectors are commercially available, ranging from thin crystals for x-ray measurements to large crystals with multiple phototubes. Crystals built with a well to allow nearly spherical 4π geometry counting of weak samples

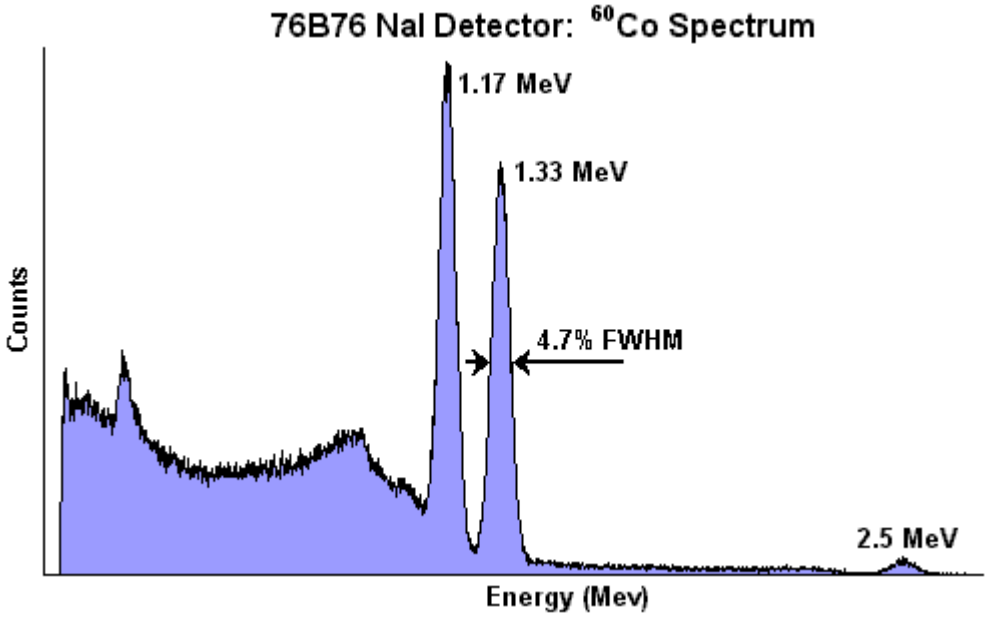

Figure 9. Typical NaI spectrum for a ^{60}Co source.

2. Other scintillators – other scintillator materials in common use are listed in Table 1 where their properties are compared to NaI. They have poorer resolution than NaI but have higher detection efficiency. A typical CsI spectrum is shown in Figure 10, and a comparison of BGO and NaI spectra is shown in Figure 11.

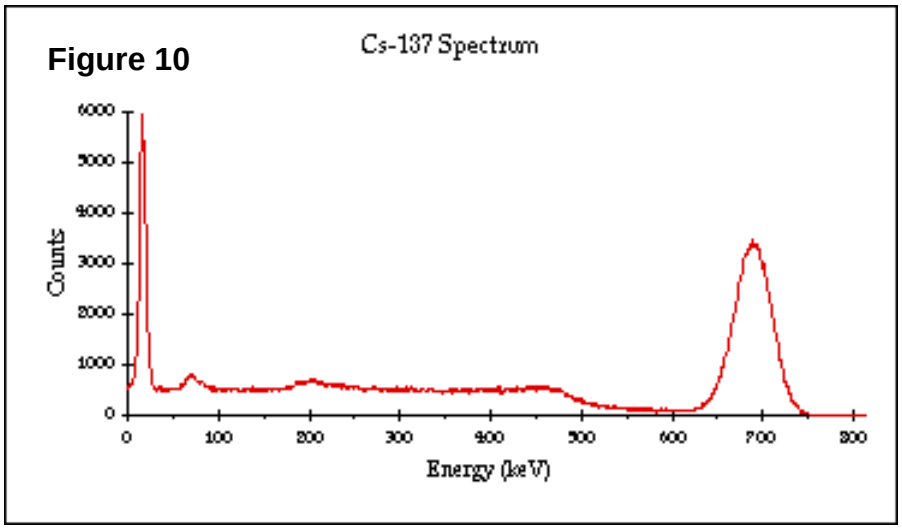

Figure 11

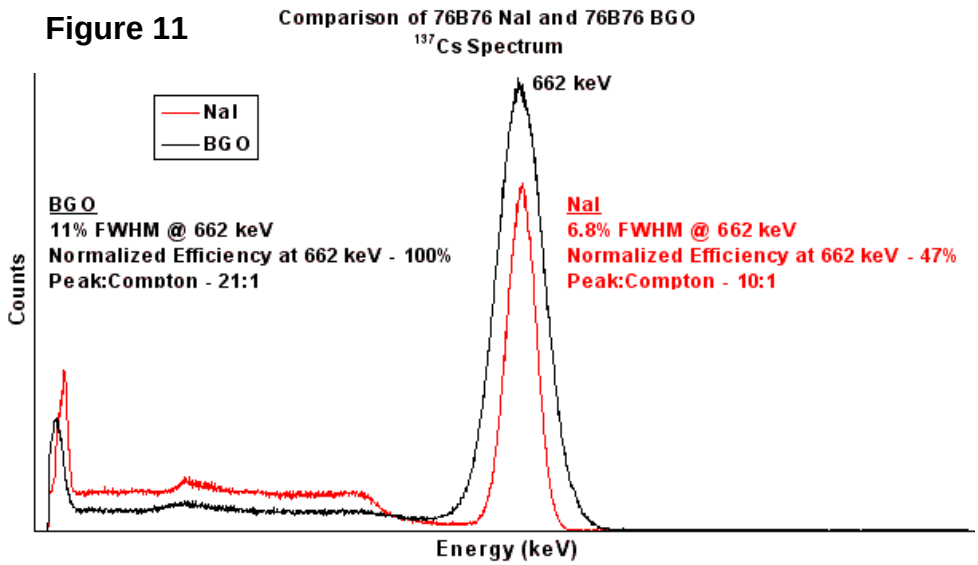

Table 1. Comparison of scintillator materials

	BaF_2	**BGO**	**CsI:Tl**	**CsI:Na**	**NaI:Tl**
Radiation Length [cm]	1.13	1.12	1.86	1.86	2.59
Relative Light Output [%]	10	8	45	85	100
Decay Constant(s) [ns]	620 / 0.6	300	≈900	630	630
Photons / MeV at 20°C	6.5 / 2000	500-1000			4000
Emission Wavelength(s)	310 / 220	480	520	520	400
Mechanical / Thermal Stability	good cleavage	good	very good	very good	fair cleavage
Radiation Resistance	very good	medium	fair	fair	fair
Hygroscopic	No	No	Slightly	Yes	Yes
Density [g/cm^3]	4.9	7.13	4.5	4.5	3.7

B. Semiconductor detectors – A semiconductor detector is fabricated from either elemental or compound single crystal materials having a band gap in the range of approximately 1 to 5 eV. The group IV elements Silicon and Germanium are the most commonly used semiconductors, although compound semiconductor materials are finding use in special applications as development work on them continues.

Table 2 shows some of the key characteristics of semiconductors detector materials. These detectors provide much better energy resolution than scintillators. This can be attributed to the small amount of energy required to produce a charge carrier and the subsequent large output signal. Only 3 eV is required to produce an electron-hole pair in Ge. The number of charge carriers produced in Ge is one or two orders of magnitude higher than for scintillation detectors. The charge multiplication that takes place in the electron multipliers associated with scintillation detectors boosts the signal but does nothing to improve the fundamental statistics of charge production.

Table 2. Semiconductor detector properties

Semiconductor	Z	Band Gap(eV)	Energy/e-h pair (eV)
Si	14	1.12	3.61
Ge	32	0.74	2.98
CdTe	48,52	1.47	4.43
HgI_2	80,53	2.13	6.5
GaAs	31,33	1.43	5.2

Semiconductor detectors have a P-I-N diode structure in which the intrinsic (I) region is created by depletion of charge carriers when a reverse bias is applied across the diode. When photons interact within the depletion region, charge carriers (holes and electrons) are freed and swept to their respective collecting electrode by the electric field. The resultant charge is integrated by a charge sensitive preamplifier and converted to a voltage pulse with amplitude proportional to the original photon energy. The depletion depth is inversely proportional to net electrical impurity concentration, and since counting efficiency is also dependent on the purity of the material, large volumes of very pure material are needed to ensure high counting efficiency for high energy photons. Prior to the mid-1970's the required purity levels of Si and Ge could be achieved only by counter-doping P-type crystals with the N-type impurity, lithium, in a process known as lithium-ion drifting. This process is still widely used in the production of Si(Li) X-ray detectors, but it is no longer required for germanium detectors since sufficiently pure crystals have been available since 1976.

1. Detector cooling - The band gap figures in Table 2 signify the temperature sensitivity of the materials and the practical ways in which these materials can be used as detectors. Ge detectors have much lower maximum operating temperatures than Si detectors. Both Ge and Si photon detectors must be cooled in order to reduce the thermal charge carrier generation (noise) to an acceptable level. The most common medium for detector cooling is liquid nitrogen; however, recent advances in electrical cooling systems have made

electrically refrigerated cryostats a viable alternative for many detector applications. In liquid nitrogen (LN) cooled detectors, the detector element (and in some cases preamplifier components), are housed in a clean vacuum chamber that is attached to or inserted in a LN Dewar. The detector is in thermal contact with the liquid nitrogen that cools it to around 77 °K or –200 °C. At these temperatures, reverse leakage currents are in the range of 10^{-9} to 10^{-12} amperes. In electrically refrigerated detectors, both closed-cycle Freon and helium refrigeration systems have been developed to eliminate the need for liquid nitrogen. Besides the obvious advantage of being able to operate where liquid nitrogen is unavailable or supply is uncertain, refrigerated detectors are ideal for applications requiring long-term unattended operation, or applications such as undersea operation, where it is impractical to vent LN gas from a conventional cryostat to its surroundings. A cross-sectional view of a typical liquid nitrogen cryostat is shown in Figure 12.

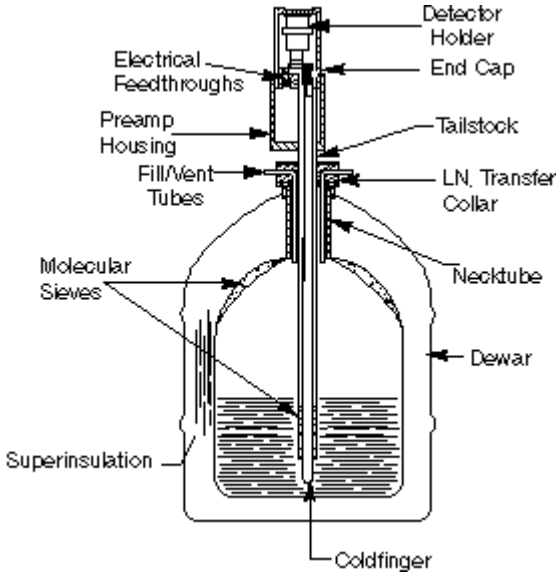

Figure 12. Typical vertical dipstick cryostat

2. Detector structure - The first semiconductor photon detectors had a simple planar structure similar to their predecessor, the Silicon Surface Barrier (SSB) detector. Soon the grooved planar Si(Li) detector evolved from attempts to reduce leakage currents and thus improve resolution. The coaxial Ge(Li) detector was developed in order to increase overall detector volume, and thus detection efficiency, while keeping depletion (drift) depths reasonable and minimizing capacitance. Other variations on these structures have come, and some have gone away, and there are several currently in use as illustrated in Figure 13.

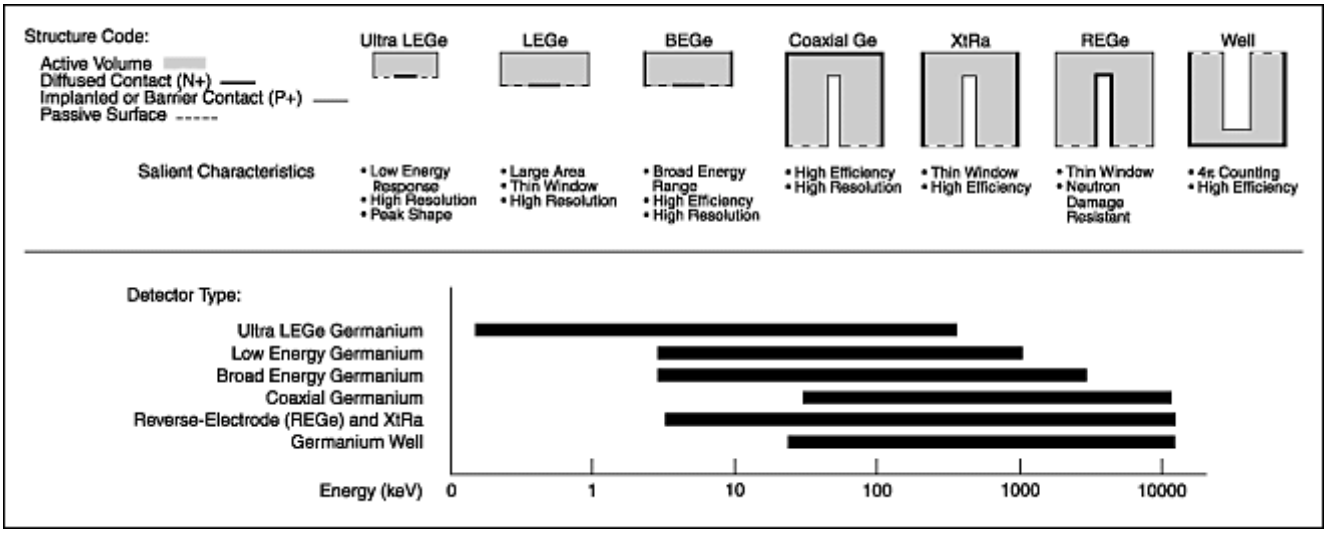

Figure 13. Common Ge detector configurations

Depending on the type of material used (N or P), the contacts are applied differently as shown in Figure 14. For P-type material, the thick, lithium contact is on the outer surface and the thin, ion-implanted contact is on the inside. For N-type material the contacts are reversed. The P-type coaxial detector is most commonly used in counting laboratories. The N-type coaxial detector has extended low-energy efficiency because of the thin contact and has slightly worse resolution specifications at higher energies.

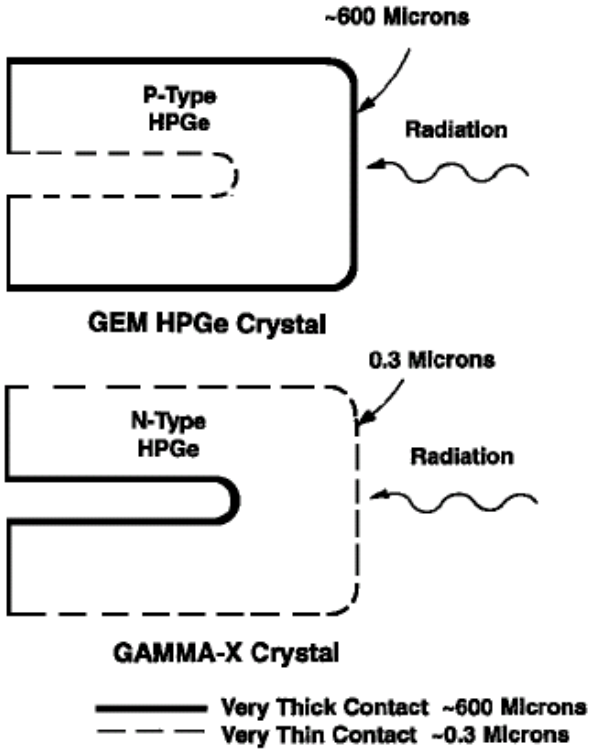

Figure 14. P- and N-type detectors

3. Detector Performance - Semiconductor detectors provide greatly improved energy resolution over other types of radiation detectors. The resolution advantage can be attributed to the small amount of energy required to produce a charge carrier and the consequent large "output signal" relative to other detector types for the same incident photon energy. The resultant energy reduction in keV (FWHM) vs. energy for various detector types is illustrated in Table 3.

Table 3. Comparison of energy resolution for various detectors.

Detector	**Resolution (keV) fwhm**		
Energy (keV)	5.9	122	1332
Proportional Counter	1.2	----	----
X-ray NaI(Tl)	3.0	12.0	----
3 x 3 NaI(Tl)	----	12.0	50
Si(Li)	0.16	----	----
Planar Ge	0.18	0.5	----
Coaxial Ge	----	0.8	1.8

At low energies, detector efficiency is a function of cross-sectional area and window thickness while at high energies total active detector volume mostly determines counting efficiency. Detectors having thin contacts, e.g. Si(Li), Low-Energy Ge and Reverse Electrode Ge detectors, are usually equipped with a Be cryostat window to improve low-energy response. Coaxial Ge detectors are typically specified in terms of their relative full-energy peak efficiency compared to that of a 3x3 in. NaI(Tl) Scintillation detector at a detector to source distance of 25 cm. Detectors of greater than 100% relative efficiency have been fabricated from germanium crystals ranging up to about 75 mm in diameter and weighing about 2 kg.

C. Segmented and clover HPGe Detectors – in recent years multiple HPGe detectors have been packaged in a single cryostat. This tends to lower detector cost because smaller detectors are less expensive to produce than large ones. Their advantage over separate individual detectors is that coincident Compton scattering from detector to detector can be added back to the spectrum, due to their close proximity, gaining extra overall efficiency. Segmented HPGe detectors are divided into separate electronically isolated sections providing higher granularity for applications where position information is important. Highly segmented strip Germanium detectors can provide excellent position information for x-rays or low-energy γ-rays. Examples of clover detectors, some with segmentation, are shown in Figure 15.

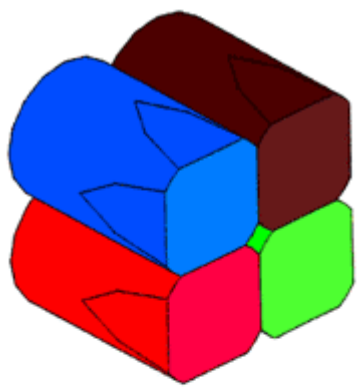

EUROGAM CLOVER

^{60}Co	FWMH	: 4 x 2,15 keV
	εr	: 4 x 20%
	εr add-back	: 130%

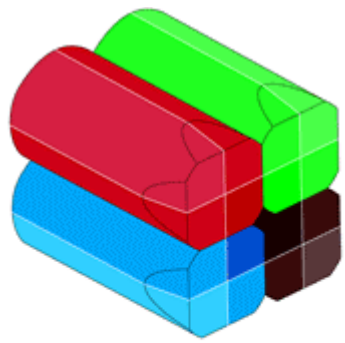

4 FOLD SEGMENTED SUPER CLOVER

Arrangements of 4 detectors 140 mm long

4 Full Volume FWMH : 2,6 keV to 1,33 MeV
9 Position FWMH : 3.2 keV to 1,33 MeV

Figure 15. Examples of clover HPGe detectors courtesy of Canberra Industries Inc.

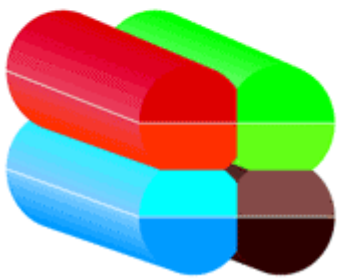

2 FOLD SEGMENTED CLOVER

^{60}Co	FWHM	: 4 x 2,25 keV
	εr	: 4 x 22%

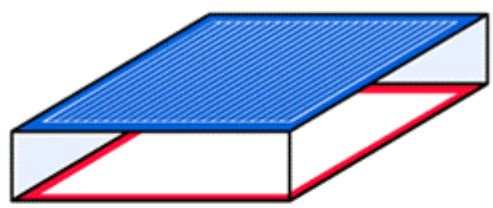

STRIP GERMANIUM DETECTOR

FOR X-Y MEASUREMENTS

Long. = 50 mm Width = 50 mm Thick. = 10 mm

2 x 25 strips: FWHM = 1.3 keV at 662 keV
Pitch = 2 mm

(X-γ imaging, γ tracking)

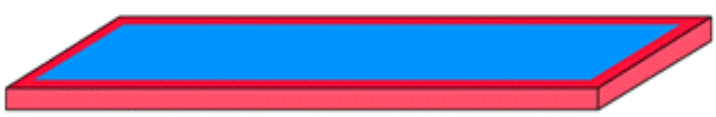

STRIP GERMANIUM DETECTOR

864 strips - 350 μ pitch

Long. = 150 mm Width = 20 mm Thick. = 2 mm

FWHM = 1.3 keV at 60 keV

(angiography)

4. Compton Suppression Systems

A limit to the detection sensitivity of any detector system is the background produced by partial absorption of the gamma ray in the detector. The background under a gamma ray peak contains no useful information. Uncertainty in the analysis of peak area is approximately equal to

$$[A(peak)+2\times A(Bkg)]^{1/2}$$

Where *A(peak)* and *A(Bkg)* are the peak and background areas respectively. Clearly reduction of the background will improve the sensitivity to weak gamma rays.

Compton suppression systems can be constructed by surrounding the detector with scintillator material, typically NaI, CsI, or BGO. The source must be outside the Compton suppressor and collimated so that no gamma rays can enter the scintillator. The gamma-ray spectrum is then counted in anti-coincidence mode to remove any events that leave energy in the scintillator. In addition to removing the Compton scattering background, Compton suppression will also reduce single and double escape peaks from pair production. A well designed Compton suppressor will decrease the background by a factor of 10 and improve sensitivity by a factor of 3. A typical Compton suppression system is shown in Figure 16, and a comparison of a Compton suppressed spectrum to an unsuppressed spectrum is shown in Figure 17.

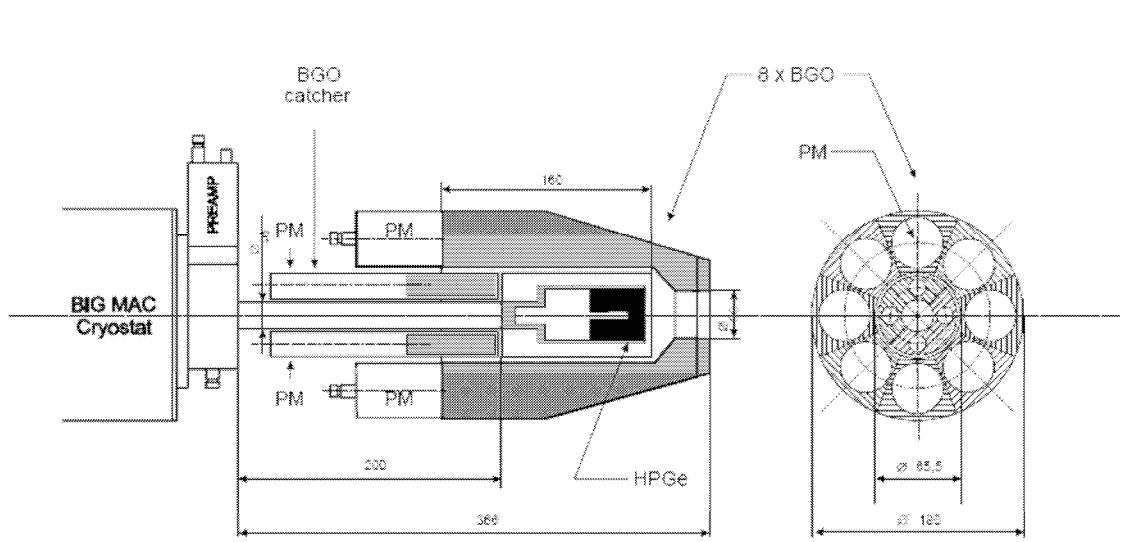

Figure 16. Budapest Compton-suppressed spectrometer.

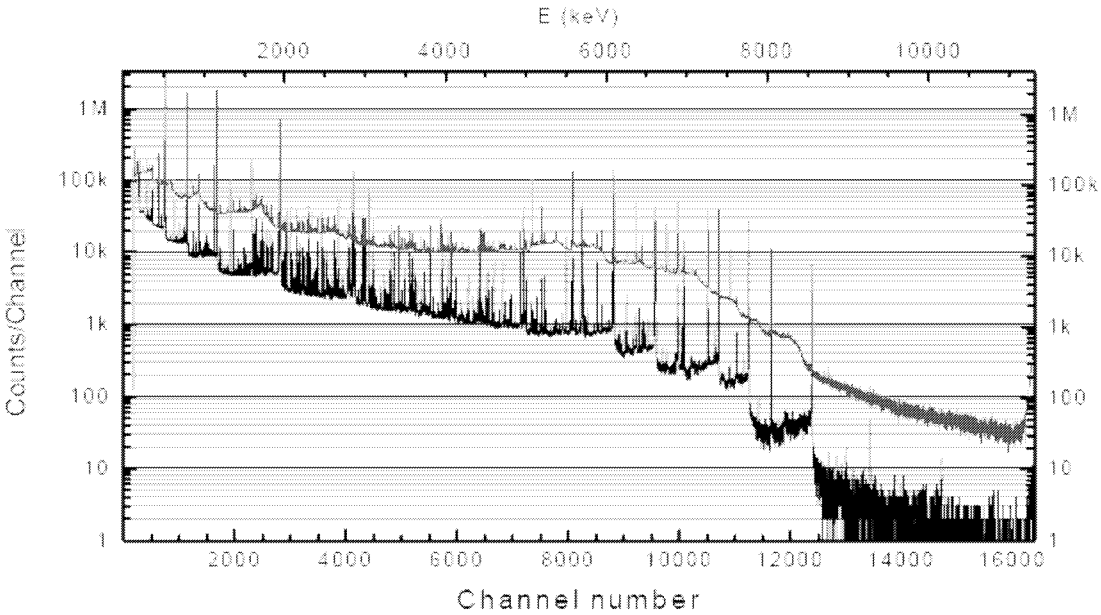

Figure 17. Ungated and Compton suppressed spectra of CCl_4 sample.

4. Germanium Detector Calibration

A. Energy calibration – all γ-ray energy standards are related to the energy of the 411.8-keV transition from ^{198}Au decay which in turn is related to the mass of the electron. This energy standard has varied considerably over time as shown in Table 4.

Table 4. Variation of 411.8-keV γ-ray energy over time.

Year	Energy(keV)
1964	411.795±0.009
1977	411.80441±0.00015
2004	411.80205±0.00017

Larger variations are reported in different measurements of standard calibration sources that are compounded by changes in the gold standard calibration energy. It is recommended that NAA researchers avoid using energies from the literature, or older compilations, and instead use the most recent γ-ray energy evaluation[2]. Appendix I gives a list of recommended energy calibration values[3]. An energy calibration curve relating the energy E to the analyzer channel number C can be represented by a simple polynomial of the form

$$E = a_0 + a_1C + a_2C^2$$

where a_0, a_1, and a_2 are parameters determined by a numerical fit to the data.

For most applications, including NAA, high precision energy calibration is not required because the energies are used solely to identify the γ-rays. It is important, particularly when analyzing the unknown samples, to calibrate with sufficient precision to avoid the misidentification of γ-rays from different sources with similar energies.

B. Efficiency calibration

A good efficiency calibration is extremely important for Neutron Activation Analysis measurements. The standard procedure for efficiency calibration is to measure a relative efficiency curve using several standard sources, and then measures the absolute efficiency with a well-calibrated standard. Appendix I lists the recommended emission probabilities for several sources.

The relative efficiency at a given γ-ray energy is $\varepsilon(E_\gamma)=A/P_\gamma$ where A is the observed peak area and P_γ is the absolute emission probability. The efficiency calibration curve is more difficult to construct than the energy calibration curve because the efficiency increases with decreasing energy until detector window thickness begins to reduce the efficiency. Typical detector efficiency curves peak at about 100 keV.

Molnar *et al* [3] showed that for a narrow energy range a good efficiency curve could be generated by assuming that the efficiency is inversely proportional to the power of γ-ray energy, i.e.

$$\varepsilon = a_1(E/E_0)^{-a2}$$

where $a_2 \approx 1$ and E_0 is an arbitrary energy that makes the argument dimensionless. This can be generalized to a larger energy range by the polynomial expansion

$$\ln \varepsilon = a_1(\ln E) + a_2(\ln E)^2 + a_3(\ln E)^3 + a_4(\ln E)^4 + a_5(\ln E)^5 + \ldots$$

where a_i are adjustable parameters. Order of the polynomial is selected by statistical criteria. Data for each calibration source are fit to a separate polynomials and the data are combined by a least-squares fit renormalization of the separate fits. Details of this analysis are discussed in reference 4 where accuracies better than 0.5% were obtained for E_γ between 100-3500 keV. A typical efficiency curve for a 25% HPGe coaxial detector with fitting parameters as discussed above is shown in figure 18.

Figure 18. HPGe 25% coaxial detector efficiency curve.

Clover and 25% coaxial detector efficiency curves are shown in figure 19. Although the clover has approximately four times the volume of the coaxial detector, it is about ten times as efficient at high energies when Compton scattering is added back.

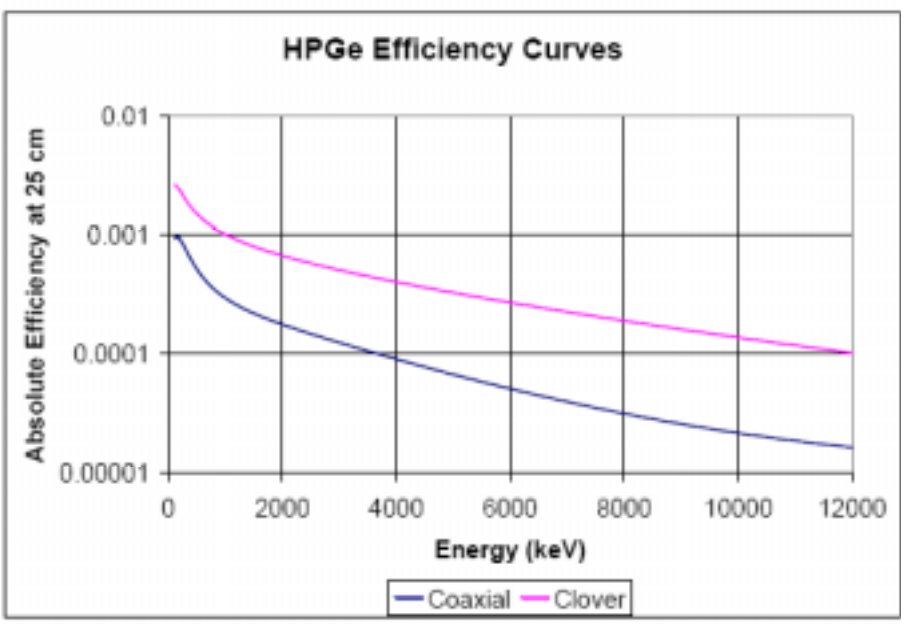

Figure 19. Comparison of clover and coaxial detector efficiency curves.

C. Spectrum Analysis Software

Gamma-ray spectra can be complex, particularly when numerous decay sources are present as is often the case with NAA. Analysis of γ-ray peak centroids and areas can be complex and has been the subject of much research. Figure 20 shows an example of a particularly complex spectrum containing 8 overlapping peaks. Spectrum analysis codes assume various algorithms for the peak shapes, typically including a Gaussian shape for the main peak with exponential tails on one or both sides. Inspection of the background under the large peak at the right shows how it evolves through the peak. Simple integration of a peak by drawing a straight background through the endpoints would be less accurate.

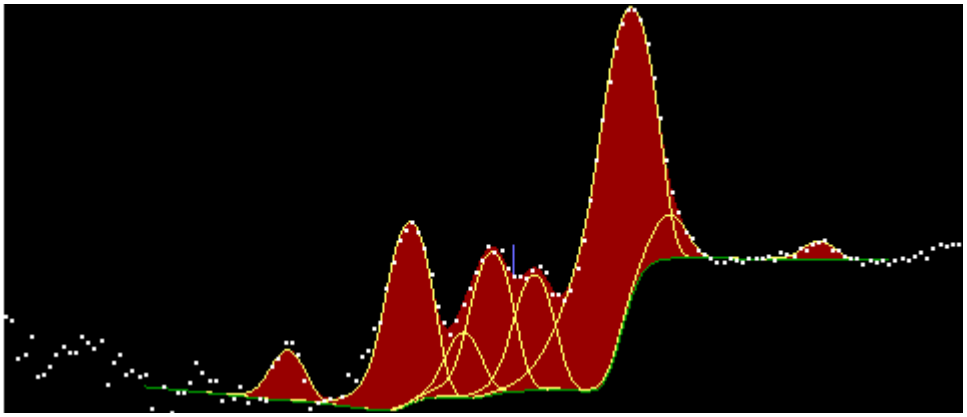

Figure 20. Complex region of a γ-ray spectrum. A total of 8 peaks were fit using the analysis program Hypermet[4].

No functional form for the peak shape will be exact, and peaks with high statistics will tend to fit poorly as systematic errors dominate.

An IAEA intercomparison of γ-ray spectrum analysis software was performed in 1995[5]. They found that the uncertainties in peak centroids tended to be underestimated and the fitting of close doublets was often lacking in statistical control. Unbiased peak areas agreed within 1%, although it is reasonable to expect that relative peak areas with common systematic errors would be more precise. It is important to conservatively estimate uncertainties in γ-ray analysis. The precision in peak intensities should not be better that the precision in the efficiency curve, typically >0.5%. Limits in precision of the energy centroid are harder to estimate because while the standards are extremely precise, small nonlinearities in the ADC are hard to determine. As a rule, energies measured with HPGe detectors should be considered no more precise than 10 eV.

D. Special circumstances.

Normal fitting procedures do not apply to some γ-ray peaks due to special circumstances.

511 keV annihilation peak – The annihilation of positrons produced by $\beta+$ decay or pair production occurs in positronium, a system in which the positron is in motion. This leads to a Doppler broading of the 511 keV annihilation radiation which must be fit with a separate function. The 511-keV intensity cannot be used for analysis because it varies depending on the material that the positron annihilates into.

X-rays – these radiations are composites of several transition groups, i.e. K_α, K_β, L_α, L_β, L_γ, which may be difficult to resolve. The relative intensities of the K x-ray groups are well known and a constrained fit fixing the intensities can be used to accurately fit several groups simultaneously[6]. Weak x-ray intensities may be unreliable due to x-ray fluorescence of the sample.

Natural line width – γ-rays from nuclear levels with very short lifetimes will have natural line broadening due to the uncertainty principal. This is seldom a problem for NAA.

Doppler broadening – the γ-ray width will be broadened if emitted from a moving source. This may occur for direct reactions or in-beam measurements. Some broadening can, in principle, occur from beta recoils. The 480 keV γ-ray used for boron analysis in PGAA is produced by the $^{10}B(n,\alpha)$ reaction and is substantially broadened.

Sum peaks –γ-rays can sum in two ways. Accidental summing occurs when two γ-rays accidentally arrive nearly simultaneously in the detector. Coincident summing occurs when two coincident γ-rays from the same decay strike the detector simultaneously. Accidental summing depends on the count rate and signal processing time. Coincident summing is independent of count rate, but depends on how close the source is to the detector. If the sum peak energy corresponds to the energy of a real peak in the decay, it must be corrected for.

Escape peaks – high energy γ-rays that interact by pair production will produce escape peaks at E_γ-511 and E_γ-1022 keV when the positron annihilation radiation escape the detector. Low energy transitions may produce Ge escape peaks at E_γ-10 and E_γ-11 keV when Ge x-rays produced during Rayleigh scattering escape the detector.

Source attenuation – absorption of the γ-ray in the source can be a major cause of error. This is particularly a problem for low energy γ-rays and/or thick sources. In some cases attenuation can be detected by comparing the analytical results as a function of energy from a multiline source. Spectroscopists should always look out for attenuation affects and avoid using low-energy γ-rays or x-rays whenever possible. Corrections for attenuation can be made with computer codes such as XCOM, available from National

Institute of Standards and Technology (NIST) at
http://physics.nist.gov/PhysRefData/Xcom/Text/XCOM.html[1].

III. Physics of Activation Analysis

Gamma rays detected in Neutron Activation Analysis normally result from the decay of radioactive products producing by neutron capture. Analysis of these data requires knowledge of the production cross-section or k_0, the half-life, and the isotopic abundance of the capturing isotope.

A. Decay schemes

The γ-rays emitted in nuclear decay de-excite the levels of the daughter nucleus which are populated by α,β-decay. Most NAA practitioners use k_0 factors recommended by experts in the field. Additional information can be obtained from the well-known relative intensities in the decay scheme. As an example, Figure 21 shows the decay scheme for ^{75}Se (119.8 d).

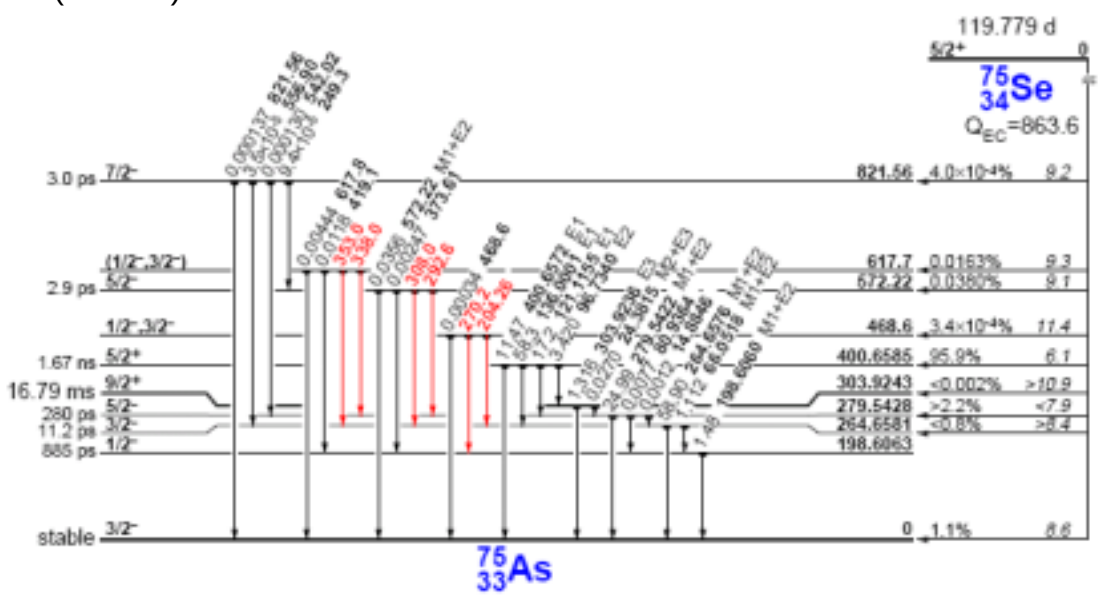

Figure 21. ^{75}Se decay scheme from the *Table of Isotopes (1999)*[7].

Things to note from this decay scheme are that the decay energy is too low for positron emission so no 511-keV radiation can be produced from this decay, and there are many coincidence γ-rays suggesting that summing could be a problem. The 303.9-keV level is a short-lived isomer, and γ-rays feeding that level won't generally coincident sum.

Table 5 compares ^{75}Se data from the K_0 website[8] with that from DDEP[9]. Data from the K_0 website have no uncertainties, and the γ-ray transition probabilities often disagree outside of the uncertainties of reference 10. The K_0 data contain cross section information not necessarily included in the evaluated decay data. It is apparent that a

new, combined evaluation of these data could benefit both areas. Meanwhile, NAA users should look at both sources of information when estimating their uncertainties.

Table 5. Comparison of data from the DDEP[10] and the K_0 website[9]

E_γ	K_0	$P_\gamma(K_0)$%	P_γ(TOI)%
66.0518(6)			1.112(12)
96.7340(9)	4.27E-04	3.481	3.42(3)
121.1155(11)	1.98E-03	17.32	17.2(3)
136.0001(8)	6.89E-03	58.98	58.2(7)
198.6060(12)	1.80E-04	1.472	1.48(4)
264.6576(9)	7.25E-03	59.1	58.9(3)
279.5422(10)	3.06E-03	25.18	24.99(13)
303.9326(10)	1.64E-04	1.342	1.316(8)
400.6572(8)	1.45E-03	11.56	11.47(9)

B. Half-lives

The analysis of NAA data frequently requires measuring γ-rays from nuclides with varying half-lives that must be analyzed at different times. It has been observed that precise half-lives do not generally agree with each other within their uncertainties. Nobody knows why this occurs. An example for ^{137}Cs is shown in Figure 22. Measurements reported with a precision of 0.05% differ by as much as 3%. Similar problems are seen for many other cases and there is no adequate method to represent this variation in the recommended uncertainties. Users are especially forewarned to be wary of very precise half-life values based on a single measurement.

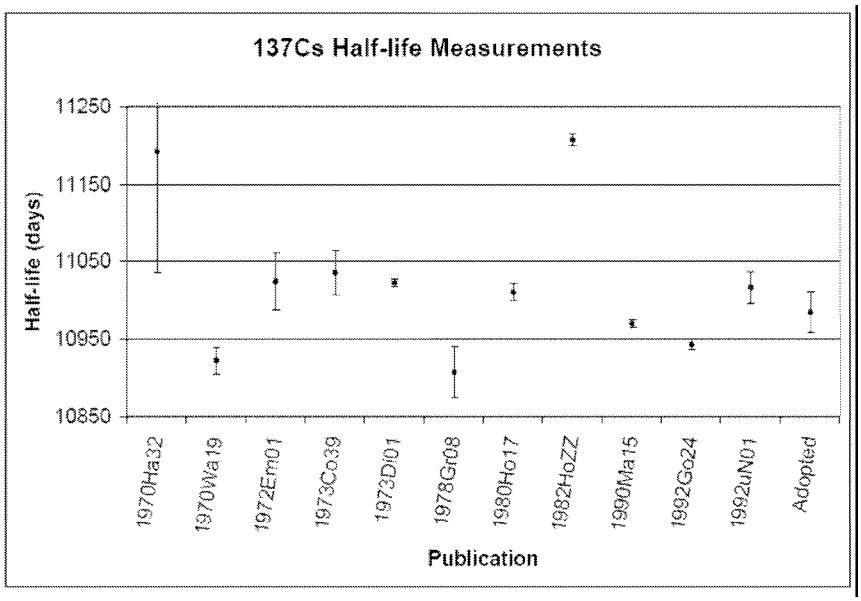

Figure 22. Distribution of half-life measurements for ^{137}Cs

Half-life variations may be due to unknown experimental errors or sample environment. It is well known that electron capture decay rates can change depending on the chemical environment. This is most notable under extreme conditions, and thought to be limited to about 0.1% uncertainty. Larger affects, of order a few percent, are observed in the low energy IT decay of ^{235m}U by changing the chemical conditions[10]. Alpha decay rates are shown to vary by 0.01% in different chemical environments[11]. Atomic affects typically contribute to about 1% of the beta decay wavefunctions, and a difference of 10 eV in molecular binding energies should affect a 100 keV Q-value beta decay by about 0.05 percent. It is prudent not to trust half-lives more precise than 0.1 %.

C. Isotopic Abundance

Isotopic abundance can play an important role in Neutron Activation Analysis. Appendix II provides the IUPAC recommended isotopic abundances[12]. Natural abundance is implicit in the k_0 tables because in many cases only one isotope of an element is actually analyzed. Uncertainty in k_0 must reflect the uncertainty in the isotopic abundance in the material analyzed. Similarly, NAA users must account for the uncertainty in the isotopic abundance in the material that they analyze.

The uncertainties shown in Appendix II are supposed to cover the range of probable variations of the materials and experimental errors. Other tables may show the uncertainty in the best measurement from a single terrestrial source. That uncertainty is not typical and should not be used. The representative uncertainties in Appendix II are only a guideline, and there is often too little experimental data to know how extensive they may be. Some examples of special problems follow.

1. ^{36}S – this isotope is an attractive candidate for the activation analysis of sulfur because ^{37}S has a short half-life (5 m) and emits readily detected γ-rays. However, the reported abundance has a 50% uncertainty because the range of natural abundance varies widely. NAA can be used in conjunction with other techniques to measure the abundance of ^{36}S in a sample, but it cannot be used for sulfur analysis.
2. ^{65}Cu – the representative abundance of ^{65}Cu is reported as 30.83 *3* with an 0.1% uncertainty. The range of natural variations is 30.89 *13* or 0.4% uncertainty. The representative uncertainty may by smaller than the range of natural variations. This may also be true of other isotopes.
3. Pb – all of the lead isotopes are reported with representative uncertainties of 0.1% which is common for most commercial samples. The range of natural variation is about 25% for ^{204}Pb, 10% for $^{206,207}Pb$, and 6% for ^{208}Pb.
4. ^{234}U – the abundance of ^{234}U is calculated from the decay of ^{238}U decay chain. It is produced from the decay of ^{234}Th that has a 24 d half-life. The actual abundance of ^{234}U in any sample can vary widely because of the mobility of ^{234}Th after it is produced by alpha decay of ^{238}U. This abundance cannot be used for analysis.
5. ^{235}U – the abundance of this isotope is remarkably constant in nearly all samples. However, substantial depletion has been observed in the Oklo natural reactor, and other cases may exist. Modern uranium may also come from reprocessed sources with anomalous depletion.

Appendix I. Recommended γ-ray calibration energies and intensities*.

Parent	E_γ(keV)[1]	I_γ(%)[2]
^{7}Be(53.22 d)		
	477.6035 *20*	10.44 *4*
^{22}Na(2.602 y)		
	1274.537 *7*	99.935 *15*
^{24}Na(14.959 h)		
	1368.626 *5*	99.9935 *5*
	2754.007 *11*	99.872 *8*
^{46}Sc(83.79 d)		
	889.271 *2*	99.9833 *5*
	1120.537 *3*	99.986 *36*
^{51}Cr(27.70 d)		
	320.0824 *4*	9.87 *5*
^{54}Mn(312.12 d)		
	834.838 *5*	99.9746 *11*
^{56}Co(77,233 d)		
	846.7638 *19*	99.933 *7*
	977.363 *4*	
	1037.8333 *24*	14.13 *5*
	1175.0878 *22*	2.239 *11*
	1238.2736 *22*	66.07 *19*
	1360.196 *4*	4.256 *15*
	1771.327 *3*	15.49 *5*
	1810.726 *4*[a]	
	1963.703 *11*	
	2015.176 *5*	3.029 *13*
	2034.752 *5*	7.771 *27*
	2113.092 *6*	0.366 *6*
	2212.898 *3*	0.390 *7*
	2598.438 *4*	16.96 *6*
	3009.559 *4*[a]	0.995 *21*
	3201.930 *11*	3.13 *9*
	3253.402 *5*	7.62 *24*
	3272.978 *6*	1.78 *6*
	3451.119 *4*	0.93 *4*
^{57}Co(271.74 d)		
	122.06065 *12*	85.51*6*
	136.47356 *29*	10.71*15*
^{58}Co(70.86 d)		
	810.7593 *20*	99.45 *1*
^{59}Fe(44.495 d)		
	1099.245 *3*	56.59 *21*
	1291.590 *6*	43.21 *25*
^{60}Co(1925.3 d)		
	1173.228 *3*	99.857 *22*
	1332.492 *4*	99.983 *6*
^{65}Zn(244.06 d)		
	1115.539 *2*	50.60 *24*
^{66}Ga(9.49 h)		
	833.5324 *21*	6.03 *23*
	1039.220 *3*	37.9 *12*
	1333.112 *5*	1.23 *5*
	1418.754 *5*	
	1508.158 *7*	
	1898.823 *8*	
	1918.329 *5*	2.14 *8*
	2189.616 *6*	5.71 *21*
	2751.835 *5*	23.2 *11*
	3228.800 *6*	1.48 *12*
	3380.850 *6*	1.40 *12*
	3422.040 *8*	
	4085.853 *9*	1.14 *19*
	4461.202 *9*	
	4806.007 *9*	1.5 *4*
^{75}Se(119.78 d)		
	66.0518 *8*	1.10 *2*
	96.7340 *9*	3.41 *4*
	121.1155 *11*	17.1 *1*
	136.0001 *6*	58.8 *3*
	198.6060 *12*	1.49 *1*
	264.6576 *9*	59.0 *2*
	279.5422 *10*	25.0 *1*
	303.9236 *10*	1.31 *1*
	400.6572 *8*	11.5 *1*
^{84}Rb(32.77 d)		
	881.6041 *16*	
	1897.751 *11*	
^{85}Sr(64.84 d)		
	515.0048 *22*	98.4 *4*
^{88}Y(106.65 d)		
	898.036 *4*	93.90 *23*
	1836.052 *13*	99.32 *3*
^{94}Nb(20300 y)		
	702.639 *4*	99.79 *5*
	871.114 *3*	99.86 *5*

Appendix I, continued

Parent	E_γ(keV)[1]	I_γ(%)[2]
^{95}Zr(64.03 d)		
	724.193 *3*	44.1*20*
^{95m}Tc(61 d)		
	204.1161 *17*	
	582.0775 *21*	
	765.803 *6*	
	786.1922 *27*	
	820.622 *7*	
	835.146 *6*	
	1039.260 *6*[b]	
^{99}Mo(65.94 h)		
	40.58323 *17*	1.022 *27*
	140.511 *1*	89.6 *17*
^{106}Ru(373.59 d)		
	511.8534 *23*[c]	
^{108m}Ag(418 y)		
	433.937 *4*	
	614.276 *4*	
^{110m}Ag(249.76 d)		
	446.812 *3*	3.65 *5*
	620.3553 *17*	2.72 *8*
	657.7600 *11*	94.38*8*
	677.6217 *12*	10.56 *6*
	687.0091 *18*	6.45 *3*
	706.6760 *15*	16.48 *8*
	744.2755 *18*	4.71 *3*
	763.9424 *17*	22.31 *9*
	818.0244 *18*	7.33 *4*
	884.6781 *13*	74.0 *12*
	937.485 *3*	34.51 *27*
	1384.2931 *20*	24.7*5*
	1475.7792 *23*[b]	4.03 *5*
	1505.0280 *20*	13.16 *16*
	1562.2940 *18*	1.21 *3*
^{113}Sn(115.09 d)		
	391.698 *3*	64.89 *13*
^{124}Sb(60.20 d)		
	602.7260 *23*	98.0 *1*
	645.8520 *19*	7.3 *1*
	713.776 *4*	
	722.782 *3*	11.3 *2*
	790.706 *7*	
	968.195 *4*	

Parent	E_γ(keV)[1]	I_γ(%)[2]
^{124}Sb (continued)		
	1045.125 *4*	
	1325.504 *4*[b]	
	1368.157 *5*	
	1436.554 *7*	
	1690.971 *4*	48.5 *3*
	2090.930 *7*	5.66 *9*
^{125}Sb(2.7586 d)		
	176.314 *2*	0.190 *9*
	427.874 *4*	29.2 *3*
	463.365 *4*	10.36 *10*
	600.597 *2*	17.55 *21*
	606.713 *3*	4.96 *5*
	635.950 *3*	11.19 *12*
	671.441 *6*	1.763 *19*
^{133}Ba(3848.9 d)		
	53.1622 *6*[a]	2.14 *3*
	160.6120*16*[a]	0.638 *4*
	223.2368 *13*[a]	0.453 *3*
	276.3989 *12*	7.16 *5*
	302.8508 *5*	18.34 *13*
	356.0129 *7*	62.05 *19*
	383.8485 *12*	8.94 *6*
^{137}Cs(30.07 y)		
	661.657 *3*	85.1 *2*
^{139}Ce(137.64 d)		
	165.8575 *11*	79.87 *6*
^{141}Ce(32.508 d)		
	145.4433 *14*	48.6 *4*
^{144}Ce(284.91 d)		
	696.505 *4*	
	1185.645 *5*	
	1489.148 *3*	
^{152}Eu(13.516 y)		
	121.7817 *3*	28.41 *13*
	244.6974 *8*	7.55 *4*
	295.9387 *17*	0.442 *3*
	344.2785 *12*	26.59 *12*
	367.7891 *20*	0.862 *5*
	411.1165 *12*	2.238 *10*
	488.6792 *20*[a]	0.4139 *24*
	586.2648 *26*[a]	0.462 *4*
	678.623 *5*[a]	0.470 *4*

Appendix I**, continued**.

Parent	E_γ(keV)[1]	I_γ(%)[2]
^{152}Eu (continued)		
	778.9045 *24*	12.97 *6*
	810.451 *5*[a]	0.317 *3*
	867.380 *3*	4.243 *23*
	919.337 *4*[a]	0.429 *5*
	1085.837 *10*	10.13 *6*
	1089.737 *5*	1.73 *1*
	1112.076 *3*	13.41 *6*
	1212.948 *11*	1.416 *9*
	1408.013 *3*	20.85 *8*
	1457.643 *11*	0.498 *4*
^{153}Sm(46.284 h)		
	69.67300 *13*	4.73 *3*
	97.43100 *21*	0.772 *18*
	103.18012 *17*	29.26 *32*
	172.85307 *21*[b]	0.0737 *20*
^{153}Gd(240.4 d)		
	69.67300 *13*	2.42 *7*
	97.43100 *21*	29.0 *8*
	103.18012 *17*	21.1 *6*
	172.85307 *21*[b]	0.036 *2*
^{154}Eu(8.593 y)		
	123.0706 *9*	40.4 *5*
	247.9288 *7*	6.89 *7*
	444.4924 *19*	0.560 *8*
	591.755 *3*	4.95 *5*
	692.4205 *18*	1.79 *3*
	723.3014 *22*	20.05 *21*
	756.8020 *23*	4.53 *5*
	873.1834 *23*	12.17 *12*
	904.064 *3*	0.890 *11*
	1246.121 *4*[a]	0.862 *11*
	1274.429 *4*[b]	34.9 *3*
	1494.048 *5*	0.698 *9*
^{160}Tb(72.3 d)		
	86.7877 *3*	
	197.0341 *10*	
	215.6452 *11*	
	298.5783 *17*	
	879.378 *2*	
	962.311 *3*[b]	
	966.166 *2*[b]	

Appendix I**, continued.**

Parent	E_γ(keV)[1]	I_γ(%)[2]
^{160}Tb (continued)		
	1177.954 *3*[b]	
	1271.873 *5*	
^{161}Tb(6.906 d)		
	25.65135 *3*	
	48.91533 *5*	
	57.1917 *3*	
	74.56669 *6*	
^{169}Yb(32.026 d)		
	63.12044 *4*	44.05 *24*
	93.61447 *8*	2.571 *17*
	109.77924 *4*	17.36 *9*
	118.18940 *14*	1.87*1*
	130.52293 *6*	11.38 *5*
	177.21307 *6*	22.32*10*
	197.95675 *7*	35.93 *12*
	261.07712 *9*[b]	1.687 *8*
	307.73586 *10*[b]	10.046 *45*
^{170}Tm(128.6 d)		
	84.25474 *8*	2.48 *9*
^{172}Hf(1.87 y), ^{172}Lu(6.70 d)		
	23.9330 *2*	
	78.9422 *6*	
	81.7509 *5*	
^{182}Ta(114.43 d)		
	65.72215 *15*	
	67.74970 *10*	
	84.68024 *26*	
	100.10595 *7*	14.23 *25*
	113.67170 *22*	
	116.4179 *6*	
	152.42991 *26*	7.02 *8*
	156.3864 *3*	
	179.39381 *25*	
	198.35187 *29*	
	222.1085 *3*	7.57 *8*
	229.3207 *6*	
	264.0470 *3*	
	1121.290 *3*	35.3 *2*
	1189.040 *3*	16.42 *10*
	1221.395 *3*	27.20 *22*
	1231.004 *3*	11.57 *8*

Parent	E_γ(keV)[1]	I_γ(%)[2]
^{182}Ta (continued)		
	1257.407 *3*	
	1273.719 *3*	
	1289.145 *3*[b]	
	1373.824 *3*[b]	
	1387.390 *3*[b]	
^{192}Ir(73.827 d)		
	205.79430 *9*	
	295.95650 *15*	28.7 *1*
	308.45507 *17*	29.8 *1*
	316.50618 *17*	83.0 *3*
	416.4688 *7*	
	468.06885 *26*	47.7 *2*
	484.575 *1*	
	588.5810 *7*	4.49 *2*
	604.41105 *25*[b]	8.11 *4*
	612.46215 *26*[b]	5.28 *3*
	884.6365 *7*[b]	

Parent	E_γ(keV)[1]	I_γ(%)[2]
^{198}Au(2.6952 d)		
	411.80205 *17*	95.54 *7*
	675.8836 *7*	0.806 *7*
	1087.6842 *7*	0.159 *3*
^{203}Hg(46.612 d), ^{203}Pb(51.873 h)		
	279.1952 *10*	
	401.320 *3*	
	680.515 *3*	
^{207}Bi(32.9 y)		
	569.698 *2*	97.74 *3*
	1063.656 *3*	74.5 *2*
	1770.228 *9*	6.87 *4*
^{228}Th(1.9116 y)		
	583.187 *2*	30.6 *2*
	2614.511 *10*	35.86 *6*
^{241}Am(432.2 y)		
	26.3446 *2*	2.40 *3*
	59.5409 *1*	35.78 *9*

[1] Data from *Table of Radionuclides*, Bé M.-M., Chisté V., Dulieu C., Browne E., Chechev V., Kuzmenko N., Helmer R., Nichols A., Schönfeld E., Dersch R and from the 8th edition of the *Table of Isotopes,* R.B. Firestone, et al (John Wiley & Sons), 1996.

[a] Care may be needed in treating the spectral background due to the small peak/continuum ratio or the shape of the background.

[b] Can only be used for precise calibration at large source-detector distances so contribution from coincidence summing into this peak is negligible.

[c] Care is needed to eliminate contribution from line produced by positron annihilation.

Appendix II. Atomic abundances, uncertainties in least significant digits are shown in parentheses.

Isotope	Abundance(%)	Isotope	Abundance(%)	Isotope	Abundance(%)
^{1}H	99.9885*70*	^{38}AR	0.0632*5*	^{64}ZN	48.63*60*
^{2}H	0.0115*70*	^{40}AR	99.6003*30*	^{66}ZN	27.90*27*
^{3}HE	0.000137*3*	^{39}K	93.2581*44*	^{67}ZN	4.10*13*
^{4}HE	99.999863*3*	^{40}K	0.0117*1*	^{68}ZN	18.75*51*
^{6}LI	7.59*4*	^{41}K	6.7302*44*	^{70}ZN	0.62*3*
^{7}LI	92.41*4*	^{40}CA	96.94*16*	^{69}GA	60.108*9*
^{9}BE	100	^{42}CA	0.647*23*	^{71}GA	39.892*9*
^{10}B	19.9*7*	^{43}CA	0.135*10*	^{70}GE	20.84*87*
^{11}B	80.1*7*	^{44}CA	2.09*11*	^{72}GE	27.54*34*
^{12}C	98.93*8*	^{46}CA	0.004*3*	^{73}GE	7.73*5*
^{13}C	1.07*8*	^{48}CA	0.187*21*	^{74}GE	36.28*73*
^{14}N	99.632*7*	^{45}SC	100	^{76}GE	7.61*38*
^{15}N	0.368*7*	^{46}TI	8.25*3*	^{75}AS	100
^{16}O	99.757*16*	^{47}TI	7.44*2*	^{74}SE	0.89*4*
^{17}O	0.038*1*	^{48}TI	73.72*3*	^{76}SE	9.37*29*
^{18}O	0.205*14*	^{49}TI	5.41*2*	^{77}SE	7.63*16*
^{19}F	100	^{50}TI	5.18*2*	^{78}SE	23.77*28*
^{20}NE	90.48*3*	^{50}V	0.250*4*	^{80}SE	49.61*41*
^{21}NE	0.27*1*	^{51}V	99.750*4*	^{82}SE	8.73*22*
^{22}NE	9.25*3*	^{50}CR	4.345*13*	^{79}BR	50.69*7*
^{23}NA	100	^{52}CR	83.789*18*	^{81}BR	49.31*7*
^{24}MG	78.99*4*	^{53}CR	9.501*17*	^{78}KR	0.35*1*
^{25}MG	10.00*1*	^{54}CR	2.365*7*	^{80}KR	2.28*6*
^{26}MG	11.01*3*	^{55}MN	100	^{82}KR	11.58*14*
^{27}AL	100	^{54}FE	5.845*35*	^{83}KR	11.49*6*
^{28}SI	92.2297*7*	^{56}FE	91.754*36*	^{84}KR	57.00*4*
^{29}SI	4.6832*5*	^{57}FE	2.119*10*	^{86}KR	17.30*22*
^{30}SI	3.0872*5*	^{58}FE	0.282*4*	^{85}RB	72.17*2*
^{31}P	100	^{59}CO	100	^{87}RB	27.83*2*
^{32}S	94.93*31*	^{58}NI	68.0769*89*	^{84}SR	0.56*1*
^{33}S	0.76*2*	^{60}NI	26.2231*77*	^{86}SR	9.86*1*
^{34}S	4.29*28*	^{61}NI	1.1399*6*	^{87}SR	7.00*1*
^{36}S	0.02*1*	^{62}NI	3.6345*17*	^{88}SR	82.58*1*
^{35}CL	75.78*4*	^{64}NI	0.9256*9*	^{89}Y	100
^{37}CL	24.22*4*	^{63}CU	69.17*3*	^{90}ZR	51.45*40*
^{36}AR	0.3365*30*	^{65}CU	30.83*3*	^{91}ZR	11.22*5*

Isotope	Abundance(%)
^{92}ZR	17.15*8*
^{94}ZR	17.38*28*
^{96}ZR	2.80*9*
^{93}NB	100
^{92}MO	14.84*35*
^{94}MO	9.25*12*
^{95}MO	15.92*13*
^{96}MO	16.68*2*
^{97}MO	9.55*8*
^{98}MO	24.13*31*
^{100}MO	9.63*23*
^{96}RU	5.54*14*
^{98}RU	1.87*3*
^{99}RU	12.76*14*
^{100}RU	12.60*7*
^{101}RU	17.06*2*
^{102}RU	31.55*14*
^{104}RU	18.62*27*
^{103}RH	100
^{102}PD	1.02*1*
^{104}PD	11.14*8*
^{105}PD	22.33*8*
^{106}PD	27.33*3*
^{108}PD	26.46*9*
^{110}PD	11.72*9*
^{107}AG	51.839*8*
^{109}AG	48.161*8*
^{106}CD	1.25*6*
^{108}CD	0.89*3*
^{110}CD	12.49*18*
^{111}CD	12.80*12*
^{112}CD	24.13*21*
^{113}CD	12.22*12*
^{114}CD	28.73*42*
^{116}CD	7.49*18*
^{113}IN	4.29*5*
^{115}IN	95.71*5*
^{112}SN	0.97*1*

Isotope	Abundance(%)
^{114}SN	0.66*1*
^{115}SN	0.34*1*
^{116}SN	14.54*9*
^{117}SN	7.68*7*
^{118}SN	24.22*9*
^{119}SN	8.59*4*
^{120}SN	32.58*9*
^{122}SN	4.63*3*
^{124}SN	5.79*5*
^{121}SB	57.21*5*
^{123}SB	42.79*5*
^{120}TE	0.09*1*
^{122}TE	2.55*12*
^{123}TE	0.89*3*
^{124}TE	4.74*14*
^{125}TE	7.07*15*
^{126}TE	18.84*25*
^{128}TE	31.74*8*
^{130}TE	34.08*62*
^{127}I	100
^{124}XE	0.09*1*
^{126}XE	0.09*1*
^{128}XE	1.92*3*
^{129}XE	26.44*24*
^{130}XE	4.08*2*
^{131}XE	21.18*3*
^{132}XE	26.89*6*
^{134}XE	10.44*10*
^{136}XE	8.87*16*
^{133}CS	100
^{130}BA	0.106*1*
^{132}BA	0.101*1*
^{134}BA	2.417*18*
^{135}BA	6.592*12*
^{136}BA	7.854*24*
^{137}BA	11.232*24*
^{138}BA	71.698*42*
^{138}LA	0.090*1*

Isotope	Abundance(%)
^{139}LA	99.910*1*
^{136}CE	0.185*2*
^{138}CE	0.251*2*
^{140}CE	88.450*51*
^{142}CE	11.114*51*
^{141}PR	100
^{142}ND	27.2*5*
^{143}ND	12.2*2*
^{144}ND	23.8*3*
^{145}ND	8.3*1*
^{146}ND	17.2*3*
^{148}ND	5.7*1*
^{150}ND	5.6*2*
^{144}SM	3.07*7*
^{147}SM	14.99*18*
^{148}SM	11.24*10*
^{149}SM	13.82*7*
^{150}SM	7.38*1*
^{152}SM	26.75*16*
^{154}SM	22.75*29*
^{151}EU	47.81*3*
^{153}EU	52.19*3*
^{152}GD	0.20*1*
^{154}GD	2.18*3*
^{155}GD	14.80*12*
^{156}GD	20.47*9*
^{157}GD	15.65*2*
^{158}GD	24.84*7*
^{160}GD	21.86*19*
^{159}TB	100
^{156}DY	0.06*1*
^{158}DY	0.10*1*
^{160}DY	2.34*8*
^{161}DY	18.91*24*
^{162}DY	25.51*26*
^{163}DY	24.90*16*
^{164}DY	28.18*37*
^{165}HO	100

Isotope	Abundance(%)
^{162}ER	0.14*1*
^{164}ER	1.61*3*
^{166}ER	33.61*35*
^{167}ER	22.93*17*
^{168}ER	26.78*26*
^{170}ER	14.93*27*
^{169}TM	100
^{168}YB	0.13*1*
^{170}YB	3.04*15*
^{171}YB	14.28*57*
^{172}YB	21.83*67*
^{173}YB	16.13*27*
^{174}YB	31.83*92*
^{176}YB	12.76*41*
^{175}LU	97.41*2*
^{176}LU	2.59*2*
^{174}HF	0.16*1*
^{176}HF	5.26*7*
^{177}HF	18.60*9*
^{178}HF	27.28*7*
^{179}HF	13.629*6*
^{180}HF	35.08*16*

Isotope	Abundance(%)
^{180}TA	0.012*2*
^{181}TA	99.988*2*
^{180}W	0.12*1*
^{182}W	26.50*16*
^{183}W	14.31*4*
^{184}W	30.64*2*
^{186}W	28.42*19*
^{185}RE	37.40*2*
^{187}RE	62.60*2*
^{184}OS	0.02*1*
^{186}OS	1.59*3*
^{187}OS	1.96*2*
^{188}OS	13.24*8*
^{189}OS	16.15*5*
^{190}OS	26.26*2*
^{192}OS	40.78*19*
^{191}IR	37.3*2*
^{193}IR	62.7*2*
^{190}PT	0.014*1*
^{192}PT	0.782*7*
^{194}PT	32.967*99*
^{195}PT	33.832*10*

Isotope	Abundance(%)
^{196}PT	25.242*41*
^{198}PT	7.163*55*
^{197}AU	100
^{196}HG	0.15*1*
^{198}HG	9.97*20*
^{199}HG	16.87*22*
^{200}HG	23.10*19*
^{201}HG	13.18*9*
^{202}HG	29.86*26*
^{204}HG	6.87*15*
^{203}TL	29.524*14*
^{205}TL	70.476*14*
^{204}PB	1.4*1*
^{206}PB	24.1*1*
^{207}PB	22.1*1*
^{208}PB	52.4*1*
^{209}BI	100
^{232}TH	100
^{234}U	0.0055*5*
^{235}U	0.7200*51*
^{238}U	99.274*11*

References

[1] XCOM, a computer code by M.J. Berger and J.H. Hubbell, available from the National Institute of Standards and Technology (NIST) at http://physics.nist.gov/XCOM.

[2] *Recommended standards for γ-ray energy calibration (1999),* R.G. Helmer and C. van der Leun, Nucl. Instrum, Meth. Phys. Res. A 450, 35 (2000).

[3] *Wide energy range efficiency calibration method for Ge detectors,* G.L. Molnar, Zs. Revay, and T. Belgya, Nucl. Instrum. Meth. Phys. Res. A489, 140 (2002).

[4] *Introducing Hypermet-PC for automatic analysis of complex gamma-ray spectra*, B. Fazekas, G. L. Molnar, T. Belgya, L. Dabolczi, and A. Simonits, J. Radioanal. Nucl. Chem. **215**, 271-277 (1997).

[5] *The 1995 IAEA intercomparison of g-ray spectrum analysis software,* M. Blaauw, V. Osorio Fernandez, P. van Espen, G. Bernasconi, R. Capote Noy, H. Manh Dung, and N.I. Molla, Nucl. Instrum. Meth. A387, 416 (1997).

[6] *Decay studies of neutron deficient nuclei near the Z=64 subshell: ^{142}Dy, ^{140,142}Tb, ^{140,142}Gd, ^{142}Sm, and ^{142}Pm*, R.B. Firestone, J. Gilat, J.M. Nitschke, P.A. Wilmarth, and K.S. Vierinen, Phys. Rev. C43, 1066 (1991).

[7] R.B. Firestone, V.S. Shirley, C.M. Baglin, S.Y.F. Chu, and J. Zipkin,*Table of Isotopes CD-ROM*, John Wiley & Sons, Inc. (1999).

[8] See http://iriaxp.iri.tudelft.nl/~rc/fmr/k0www3/mainframes3.htm by M. Blaauw, B. Smodis, and P. Robouch.

[9] *Decay Data Evaluation Project (DDEP) Evaluation of ^{75}Se,* E. Browne and E. Schönfeld (2004).

[10] *Perturbation of the ^{235m}U decay rate by implantation in transition metals,* M. Neve de Mevergnies, Phys. Rev. Lett. 29, 1188 (1972).

[11] *Influence of the chemical environment on α-decay,* K. Alder, G. Baur, and U. Raff, Phys. Lett. 34A, 163 *1971).

[12] *Isotopic Compositions of the Elements,* K.J.R. Rosman and P.D.P. Taylor, Pure and Appl. Chem 70, 217 (1998).